AIMS Materials Science, 5(1): 105–115.
DOI: 10.3934/matersci.2018.1.105
Received: 30 November 2017
Accepted: 25 January 2018
Published: 31 January 2018

http://www.aimspress.com/journal/Materials

Research article

Control of the spontaneous formation of oxide overlayers on GaP nanowires grown by physical vapor deposition

Yunyan Wang, Manu Hegde, Shuoyuan Chen, Penghui Yin and Pavle V. Radovanovic*

Department of Chemistry, University of Waterloo, 200 University Avenue West, Waterloo, Ontario N2L 3G1, Canada

* **Correspondence:** Email: pavler@uwaterloo.ca; Tel: +1-519-888-4567 ext. 38144; Fax: +1-519-746-0435.

Abstract: Growth of gallium phosphide nanowires by vapor deposition of simple thermally evaporated inorganic precursors is generally accompanied by unintentional formation of thick oxide coating, which may compromise the optical and electrical properties of the nanowires. Controlling and eliminating this outer layer during thermal evaporation growth of GaP nanowires represents a barrier to simple and scalable preparation of this technologically important material. In this article, we systematically investigated the role of different parameters (temperature, hydrogen flow rate, and starting Ga/P ratio) in the synthesis of GaP nanowires, and mapped out the conditions for the growth of oxide-layer-free nanowires. Increase in temperature, hydrogen flow, and phosphorus concentration led to diminished oxide layer thickness and improved nanowire morphology. Long and straight nanowires with the near perfect stoichiometry and complete absence of oxide outer layer were obtained for 1050 ℃, 100 sccm hydrogen flow rate, and Ga/P flux ratio of 0.5. In contrast to other reports, this work emphasizes the importance of introducing hydrogen flow and excess phosphorus, which provide for reducing environment and reduced rate of the reaction of Ga with O in the growth process, respectively. The ability to control dielectric medium around GaP NWs by controlling the formation of oxide overlayer was demonstrated by Raman spectroscopy. The results of this work demonstrate a full control of the multi-parameter space in the simple, inexpensive, and scalable synthesis of GaP NWs, and may provide a guideline for rational improvement of the growth conditions for other types of semiconductor nanowires.

Keywords: III-V nanowires; physical vapor deposition; phosphide; semiconducting materials; native oxide

1. Introduction

Among various one-dimensional materials synthesized and investigated over the past two decades, III-V semiconductor nanowires (NWs) have shown particular versatility for applications in optoelectronics, including solar cells [1], light emitting diodes (LEDs) [2], lasers [3,4], photodetectors [5], and spintronic devices [6–9]. The interest in GaP NWs stems from its relatively wide band gap (2.26 eV) [10], the possibility of emitting different colors [11], and the ability to introduce both electrons and holes as majority charge carriers [12,13]. Consequently, GaP NWs have been synthesized by a variety of gas-phase methods, including physical vapor deposition (PVD) [14–17], metalorganic chemical vapor deposition (MOCVD) [11,18], molecular and chemical beam epitaxy [19,20], and more recently by solution-phase approach [21]. Majority of gas-phase preparations involve vapor-liquid-solid (VLS) mechanism, enabled by a pre-deposited metal nanocluster catalyst or self-assisted growth.

Growth of NWs by hot wall deposition of thermally evaporated GaP powder is particularly promising for commercially-relevant applications because of the relatively low cost of the starting material, simplicity, safety, compatibility with a variety of dopants, and the ability grow NWs with different morphology and on various substrates [9,22–24]. However, this method generally leads to the formation of thick oxygen-rich overlayers on the NW surface, which can be either amorphous or crystalline [14–17], and often consist of Ga_2O_3 and/or $GaPO_4$ [15,17]. The sources of oxygen are believed be the oxygen impurity in the carrier gas, residual oxygen in the reaction chamber, or oxygen adsorbed on the growth substrate or the inner wall of the reactor. While this unintentionally formed coating could potentially be used as insulating oxide layer for NW electronic devices, such as field effect transistors, the adsorbed or incorporated oxygen could also compromise the inherent electrical and optical properties of GaP NWs. The rational and consistent control of the formation of this coating layer during NW growth has not yet been achieved.

In this article, we demonstrate a facile and scalable synthesis of high-quality single crystalline GaP NWs without any oxide layers by a PVD method. By systematically exploring the effect of synthesis parameters on the structure, morphology, and composition of GaP NWs, we mapped out the conditions for the NW growth based on a simple thermal evaporation of powder precursors. We found that increase in the reaction temperature, P flux, and the amount of hydrogen in the carrier gas improve the quality of NWs, reduce the level of oxygen defects in NWs, and the thickness of the oxide coating. The optimal NW products were obtained in the relative excess of phosphorus at 1050 ℃ and with 100 sccm hydrogen flow rate. The results of this work provide a scalable, facile, and inexpensive route to controlled growth of GaP NWs free of overlayers typical for PVD growth of this material.

2. Materials and method

2.1. Gallium phosphide nanowire growth

Gallium phosphide nanowires were synthesized by the hot wall physical vapor deposition (PVD) method. All chemicals purchased from the manufacturers were used as received without any further purification. Gallium phosphide (99.99% trace metal basis, Aldrich), gallium metal (99.99%, Strem Chemicals), and phosphorous (97%, Aldrich) were used as precursors. The nanowires were grown on

Si substrates ca. 1 cm^2 in area. The substrates were washed with deionized water and ethanol, and dried in the flow of nitrogen. Gold deposited on a clean substrate was employed as the metal catalyst. An aluminum boat containing the reactants on a mica sheet was inserted into a horizontal two-inch diameter quartz gas flow tube and placed in the center of a three-temperature-zone tube furnace (zone 2). The growth substrate was placed on another aluminum boat and positioned ca. 25 cm downstream from the precursors (zone 3). Before starting the reaction, the tube was evacuated to 0.1 Torr and purged with high purity (grade 5) argon gas (100 sccm flow rate) under the pressure of 200 Torr. Thereafter, the tube was gradually heated to the desired temperature under argon gas flow. For samples synthesized under hydrogen flow, after reaching the set temperature, hydrogen gas was introduced at the desired rate while argon flow rate was adjusted to maintain the total flow rate of 200 sccm. The reaction was allowed to proceed for 90 minutes, and the pressure was maintained at 200 Torr during the reaction. Samples were allowed to naturally cool down to room temperature under argon flow.

2.2. Nanowire characterization

Powder X-ray diffraction (XRD) patterns of the nanowires on a growth substrate were recorded with INEL powder diffractometer using position sensitive detector and Cu $K\alpha_1$ radiation (λ = 1.5406 Å). Field-emission scanning electron microscopy (SEM) imaging was performed with LEO 1530 microscope with the operating voltage of 10 kV, equipped with an energy dispersive x-ray spectroscopy (EDX) detector. Transmission electron microscopy (TEM) and selected area electron diffraction (SAED) measurements were performed with a JEOL 2010F microscope operating at 200 kV. For TEM imaging and SAED the growth substrates containing NW products were sonicated in ethanol, and the obtained suspensions were deposited on a copper grid with lacey Formvar/carbon support film (Ted Pella, Inc). Raman spectra were collected with Renishaw 1000 spectrometer connected to a BH-2 Olympus microscope. The measurements were performed in confocal configuration, and the samples were excited with Millenia-pumped Tsunami laser (Spectra-Physics) tuned to 785 nm.

3. Results and discussion

Initial synthesis was performed in the excess of Ga, with the Ga:GaP flux ratio of 1:1, at 1000 ℃. The resulting product consists of a mixture of very long and curved NWs and large particles evenly distributed throughout the growth substrate (Figure 1a). The average NW length is well over 5 μm. Figure 1b shows a TEM image of a typical NW from this sample. The NW has uneven surface with occasionally large protuberances along the growth direction. Selected area electron diffraction (SAED) pattern (inset in Figure 1b) indicates that the NW grows along <111> direction, which has been confirmed for other NWs in the sample. Figure 1c shows a high-resolution TEM image of the same NW. The lattice spacing of 3.14 Å confirms the <111> growth direction. Importantly, the NW has a thick outer layer which appears to be largely amorphous. The thickness of this layer ranges from 5 to over 20 nm, which can also be observed in Figure 1b as the difference in contrast between the NW core and the outer shell layer along the NW. Elemental EDX analysis of the NW shows a significant amount of oxygen (Figure 1d), which is consistent with the previously reported conclusions that the shell is made of native oxide [14,16]. The XRD pattern of the growth

substrate also shows the peaks characteristic for β-Ga_2O_3 (blue lines in Figure 1e). Given the amorphous nature of the NW shell, the β-Ga_2O_3 reflections suggest that the particles codeposited on the growth substrate consist of crystalline Ga_2O_3. Taken together, the results in Figure 1 demonstrate the propensity of oxide formation in the process of GaP NW growth by PVD based on thermal evaporation of bulk semiconductor.

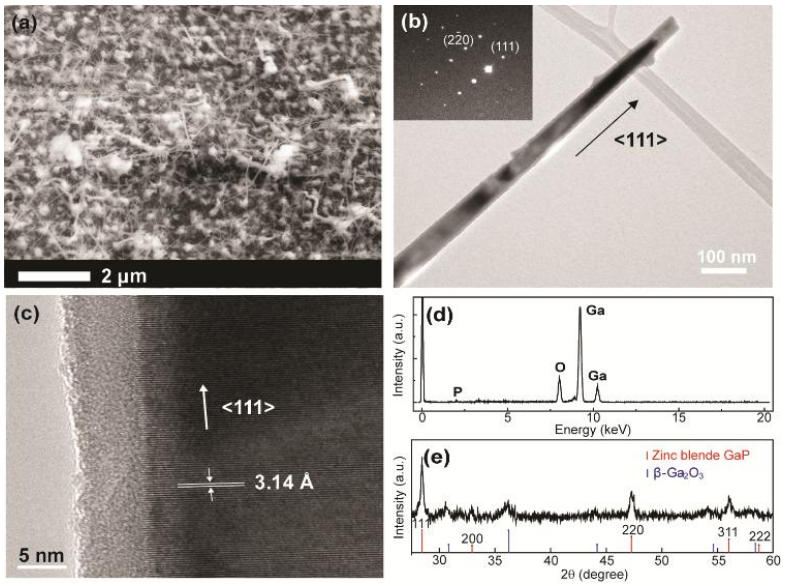

Figure 1. (a) SEM image of GaP NWs synthesized at 1000 ℃ in argon flow with excess Ga (flux ratio Ga:GaP = 1:1). (b) Typical TEM image and the corresponding SAED pattern (inset) of a single NW from (a). The arrow indicates the NW growth direction. (c) Lattice-resolved TEM image of the NW in (b). The average lattice spacing indicated in the image is consistent with <111> growth direction. (d) EDX spectrum of the NW in (b). XRD pattern of NWs on the growth substrate.

In analogy to the growth of GaN NWs [8,9], we hypothesized that the synthesis of GaP NWs in reducing conditions could minimize the effect of residual oxygen and the probability of oxide shell formation. Figures 2a–c show SEM images of the samples grown at 1050 ℃ with Ga:GaP flux ratio of 1, but with different hydrogen flow. The sample grown in the absence of hydrogen (Figure 2a) appears nearly identical to that shown in Figure 1a, as expected. A relatively moderate hydrogen flow (50 sccm) leads to a significant decrease in the amount of codeposited particles, although the NWs still have uneven surfaces or neckless-like structure with periodically spaced bumps along the NW (Figure 2b and Figure S1 in Supplementary Material) [14,16]. These bumps are found to be amorphous and oxygen-rich, indicating that native oxide overlayers are still formed during NW growth. Further increase in the hydrogen flow rate (Figure 2c) results in long and straight NWs with uniform thickness and smooth surfaces, as well as nearly complete elimination of codeposited crystalline Ga_2O_3 domains on the growth substrate. The SEM images in Figures 2a–c illustrate the evolution of NW morphology in the flow of hydrogen as a reducing agent. The NW composition (Ga/P atomic ratio and the amount of oxygen) determined by EDX measurements of individual NWs from the samples synthesized with different H_2 flow rates are summarized in Figure 2d. While the Ga/P atomic ratio gradually decreases with increasing H_2 flow rate, the amount of oxygen initially

increases followed by a sharp decrease. The initial increase in the amount of oxygen is likely due to the neckless-like morphology of NWs at moderate H_2 flow, where the bumps contain a large concentration of oxygen, despite the overall decrease in the amount of codeposited Ga_2O_3. Elimination of these bumps and the subsequent formation of straight and long NWs with smooth surfaces leads to a decrease in the amount of oxygen below 10 atom%, with the Ga:P ratio of ca. 1.2.

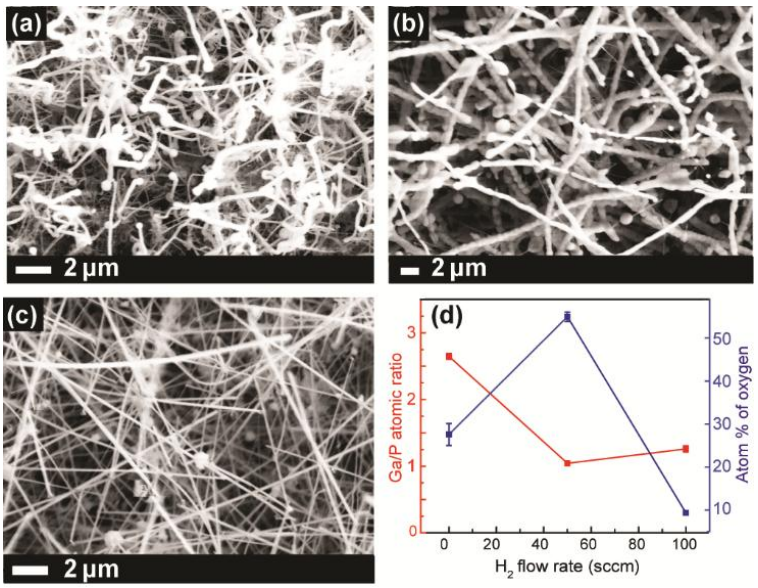

Figure 2. (a–c) SEM images of GaP NWs prepared at 1050 ℃ with flux ratio Ga:GaP = 1:1 and different hydrogen flow rates: (a) 0 sccm, (b) 50 sccm, and (c) 100 sccm. (d) Dependence of Ga/P atomic ratio (red squares) and oxygen content (blue squares) in NWs on the hydrogen flow rate.

The quantitative analysis of NWs in Figure 1a and Figure 2a, synthesized at different temperatures but otherwise under identical conditions, indicates lower concentration of oxygen in latter, suggesting that increase in temperature could also be a positive factor in eliminating the formation of oxide shell. SEM images of GaP NWs synthesized with the precursor flux ratio Ga:GaP = 1 and 100 sccm hydrogen flow at 950 ℃, 1000 ℃, 1050 ℃ are shown in Figures 3a–c, respectively. Nanowires grown at 950 ℃ show significant kinking together with a high phosphorus deficiency and oxygen content of over 40% (Figure 3d). The kinking is diminished for the sample synthesized at 1000 ℃, although NWs retain a large amount of oxygen and appear to undergo thick and uneven oxide overgrowth (Figure S2 in Supplementary Material). Importantly, the Ga:P ratio is found to approach unity. Further increase in temperature to 1050 ℃ yields straight and long GaP NWs with smooth surfaces, nearly ideal stoichiometry, and oxygen content below 10% (Figure 3d). These results clearly indicate that increasing temperature helps reduce the formation of oxide overlayers in GaP NWs.

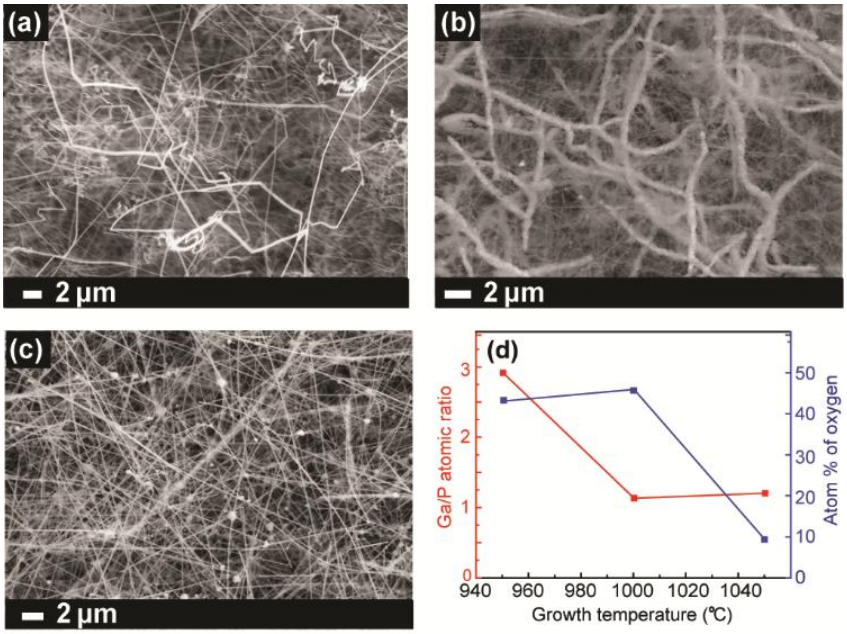

Figure 3. (a–c) SEM images of GaP NWs prepared with the flux ratio Ga:GaP = 1:1, 100 sccm hydrogen flow rate and different temperatures: (a) 950 ℃, (b) 1000 ℃, and (c) 1050 ℃. (d) Dependence of Ga/P atomic ratio (red squares) and oxygen content (blue squares) in NWs on the growth temperature.

Finally, we performed a series of growth experiments with different Ga:P ratio in the precursor mixture. Figure 4 shows the results for NWs synthesized with the optimal parameters (synthesis temperature of 1050 ℃, H_2 flow rate of 100 sccm, and the total pressure of 200 Torr) but different amounts of phosphorus in the reaction mixture. While the initial amount of phosphorus does not have a notable effect on the NW growth (Figures 4a–c) or stoichiometry (Figure 4d, red squares), an increase in the amount of phosphorus (flux ratio Ga:P = 0.5) reduces oxygen content in NWs below 1% (Figure 4d, blue squares). The nanowires in Figure 4c represent, to our knowledge, the first example of oxide-shell-free stoichiometric GaP NWs synthesized by a simple PVD method. The presence of gold particles on the tips of the vast majority of these stoichiometric oxide-free NWs, as confirmed by electron microscopy and EDX elemental line scans, strongly suggests that GaP NWs are grown by VLS mechanism. It should be noted that GaP NW growth by PVD in previously reported studies was performed in either stoichiometric amounts of Ga and P or in excess of Ga [14,15,17]. These results indicate that excess of phosphorus represents a viable approach to obtaining high quality GaP NWs that do not contain oxide overlayers.

To confirm the structure, composition, and crystallinity of individual NWs in Figure 4c, we performed TEM measurements at the single NW level. Figures 5a–b show typical EDX elemental line scan profiles of a representative NW grown at 1050 ℃, with 100 sccm hydrogen flow and the flux ratio Ga:P of 0.5. The Ga and P line scans have essentially the same form, as expected for the fully stoichiometric GaP NWs (i.e., Ga:P = 1). In contrast, the signal for oxygen is negligible across the NW. High-resolution TEM image (Figure 5c) also confirms that the oxide layer is completely removed and indicates high crystallinity along the entire NW. It is important to note that these GaP NWs remain free from any detectable oxide overlayers several weeks after the synthesis, confirming

that oxide coatings are formed almost exclusively during NW growth, rather than due to post-growth sample exposure to the atmosphere. The NW is characterized by twinning along the growth axis (Figure S3 in Supplementary Material), as observed previously in zinc blende GaP NWs [16,17,19]. It grows along <111> direction (Figure 5d), similar to NWs in Figure 1c prepared in the absence of hydrogen flow and excess of phosphorus. XRD pattern also confirm the zinc blende crystal structure and the absence of secondary crystal phases on the NW surfaces or growth substrate (Figure 5e).

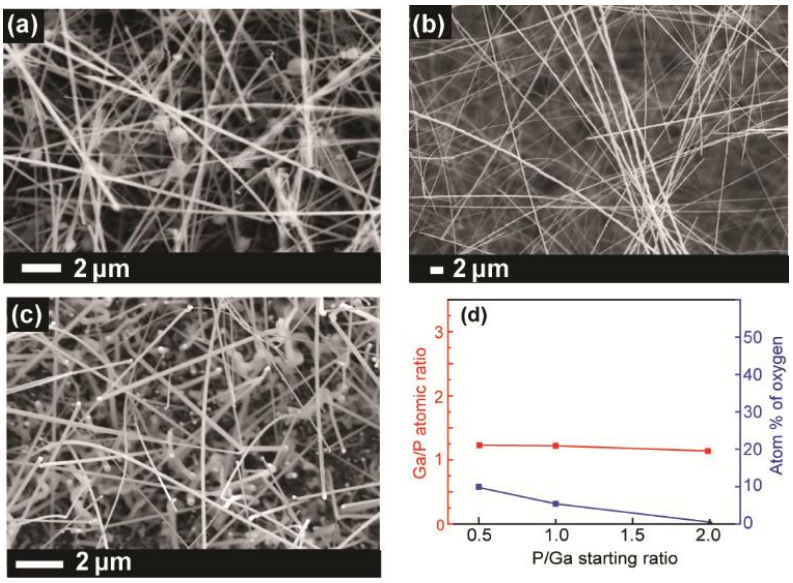

Figure 4. (a–c) SEM images of GaP NWs prepared at 1050 ℃ with 100 sccm hydrogen flow rate and Ga:P flux ratio of (a) 2:1, (b) 1:1, and (c) 1:2. (d) Dependence of Ga/P atomic ratio (red squares) and oxygen content (blue squares) in NWs on Ga:P flux ratio.

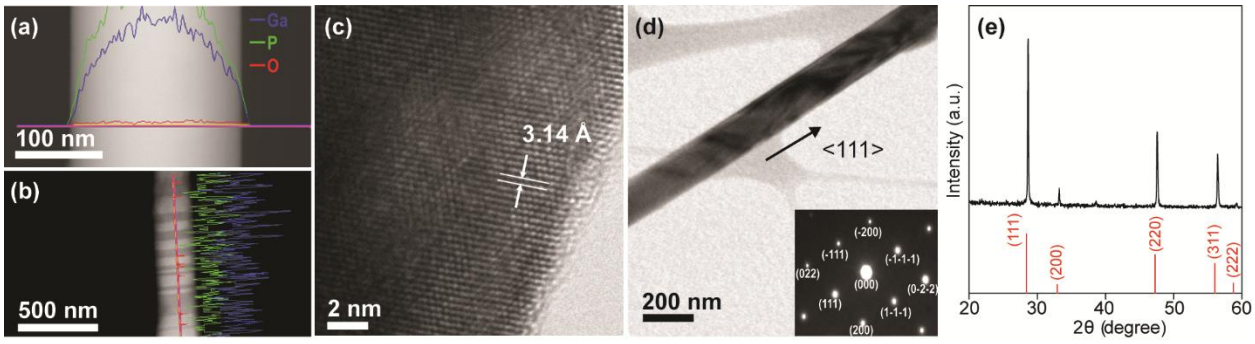

Figure 5. (a, b) EDX elemental line scan profiles of a typical GaP NW in Figure 4c (a) perpendicular and (b) along the NW growth direction (Ga, blue trace; P, green trace; and O, red trace). (b) High-resolution TEM image of NW in (a), showing an average lattice spacing corresponding to <111> plane. (d) TEM image and the corresponding SAED of the NW in (c) confirming <111> growth direction. (d) XRD pattern of GaP NWs corresponding to the SEM image in Figure 4c.

The effect of oxide coating on the NW structure and properties, and the importance of

controlling its formation were demonstrated by a series of Raman spectroscopy measurements. Figure 6 compares the Raman spectra of bulk GaP, oxide-coated NWs in Figure 1a, and GaP NWs in Figure 4c synthesized under optimized conditions. The spectrum of bulk GaP shows two characteristic peaks at 362 and 402 cm^{-1}, which can be assigned to transversal optical (TO) and longitudinal optical (LO) modes, respectively. The peaks for both TO and LO modes are broadened and shifted by ca. 4 cm^{-1} in case of NWs, indicating that the Raman spectrum is affected by one-dimensional morphology [25–27]. Importantly, the NW spectra show an additional shoulder between TO and LO bands. This new feature is assigned to surface optical (SO) phonons, which can be activated by the NW diameter modulation [25,26]. The SO band for GaP NWs has been shown to be sensitive to the dielectric constant of the surrounding medium [25]; it broadens, increases in intensity, and red shifts with increasing dielectric constant. To assess the influence of the oxide coating on the dielectric properties of GaP NWs, we deconvoluted the SO bands by fitting the Raman spectra to a linear combination of three Lorentzian functions (Figure 6, thin colored lines indicated in the graph). The SO band is found to be significantly broader and more pronounced in oxide-coated NWs (yellow traces). The center of gravity of this band also exhibits a subtle shift to lower energies, consistent with increased dielectric constant of the amorphous oxide coating relative to air. While a quantitative model for the dependence of the SO band parameters on the dielectric constant has not yet been developed, assuming similar dielectric constant of the amorphous oxide layer and crystalline Ga_2O_3, the change in the Raman spectrum of GaP NWs due to the oxide coating corresponds approximately to an increase in the dielectric constant from 1 to 10. To our knowledge, the results in Figure 6 represent the first comparison between the Raman spectra of GaP NWs with and without oxide coating, synthesized by PVD. These results suggest the GaP NW structure and properties are strongly influenced by the oxide overlayers, and emphasize the importance of controlling the formation of such coating during NW growth.

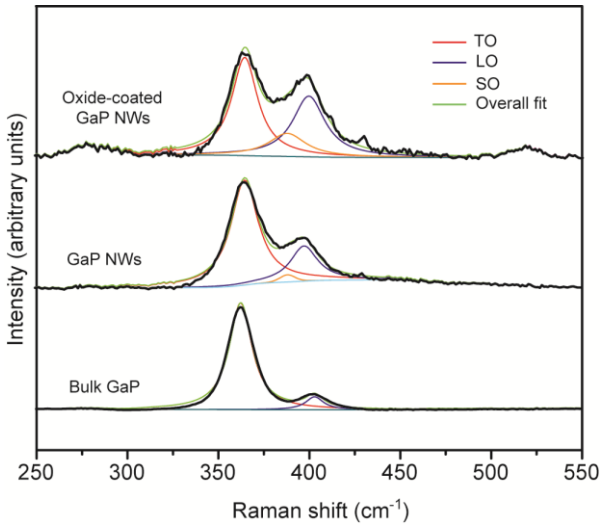

Figure 6. Raman spectra of bulk GaP (bottom), GaP NWs synthesized under optimized conditions for the removal of oxide overlayers (middle), and oxygen-coated NWs from Figure 1 (top). Raman spectra are fit to three Lorentzian functions representing TO (red line), LO (blue line), and SO (orange line) modes. Overall fit to the experimental spectra is shown with the green line.

4. Conclusions

In summary, we performed for the first time a systematic study of the growth of GaP NWs by the PVD method. We investigated the NW structure, morphology, and composition for the syntheses performed at varying growth temperature, Ga/P precursor ratio and hydrogen flow. Increase in the growth temperature, hydrogen flow rate and the amount of phosphorous in the reaction mixture were generally conducive to the preparation of long and straight NWs with nearly ideal Ga:P stoichiometry, and without the formation of Ga_2O_3 and/or $GaPO_4$ overlayers, typically observed in the PVD growth of GaP NWs. The optimal NW structure and stoichiometry were obtained for the NWs grown at 1050 ℃, with 100 sccm hydrogen flow and excess of phosphorus (Ga:P flux ratio of 0.5). Importantly, hydrogen flow, which has not been considered in the previously reported work involving PVD synthesis of GaP NWs, proved to be very effective in minimizing the formation of oxide overlayers. Furthermore, contrary to the previous reports which mostly rely on the excess Ga in the NW synthesis, the results of this work indicate the importance of excess phosphorus for obtaining high quality oxygen-free GaP NWs. The key factor in elimination of the oxide overlayers is the synthesis under reducing conditions, which is in this case ensured by the introduction of hydrogen gas flow. The excess phosphorus also helps this cause by forcing the GaP formation, and outcompeting the reaction of Ga with O in the growth process. The presence of the oxide overlayers significantly changes the dielectric constant of the surrounding medium as well as the electronic structure of the NWs, underlying the necessity of its rational control during NW growth. The results of this work allow for the simple and scalable synthesis of technologically important III-V NW system with optimal structure and composition, by chemically controlling the NW growth via control of the multi-parameter reaction space. We anticipate that the general approach and conditions in this work could be used for optimizing the structure and properties of other non-oxide-based semiconductor NWs, synthesized by PVD.

Acknowledgments

This work was supported by the Natural Sciences and Engineering Research Council of Canada (RGPIN-2015-04032), Ontario Ministry of Research and Innovation (ER10-07-104), and the University of Waterloo (UW-Bordeaux Collaborative Research Grant). P.V.R. thanks Canada Research Chairs program (NSERC) for generous support. The electron microscopy research described in this paper was performed at the Canadian Centre for Electron Microscopy at McMaster University, which is supported by NSERC and other government agencies.

Conflict of interest

The authors declare that there is no conflict of interests in this publication.

References

1. Holm JV, Jørgensen HI, Krogstrup P, et al. (2013) Surface-passivated GaAsP single-nanowire solar cells exceeding 10% efficiency grown on silicon. *Nat Commun* 4: 1498.

2. Dai X, Messanvi A, Zhang H, et al. (2015) Flexible light-emitting diodes based on vertical nitride nanowires. *Nano Lett* 15: 6958–6964.
3. Saxena D, Mokkapati S, Parkinson P, et al. (2013) Optically pumped room-temperature GaAs nanowire lasers. *Nat Photon* 7: 963–968.
4. Johnson JC, Choi HJ, Knutsen KP, et al. (2002) Single gallium nitride nanowire lasers. *Nat Mater* 1: 106–110.
5. Wang J, Gudiksen MS, Duan X, et al. (2001) Highly polarized photoluminescence and photodetection from single indium phosphide nanowires. *Science* 293: 1455–1457.
6. Hegde M, Farvid SS, Hosein ID, et al. (2011) Tuning manganese dopant spin interactions in single GaN nanowires at room temperature. *ACS Nano* 5: 6365–6373.
7. Farvid SS, Hegde M, Hosein ID, et al. (2011) Electronic structure and magnetism of Mn dopants in GaN nanowires: Ensemble vs single nanowire measurements. *Appl Phys Lett* 99: 222504.
8. Stamplecoskie KG, Ju L, Farvid SS, et al. (2008) General control of transition-metal-doped GaN nanowire growth: Toward understanding the mechanism of dopant incorporation. *Nano Lett* 8: 2674–2681.
9. Radovanovic PV, Stamplecoskie KG, Pautler BG (2007) Dopant ion concentration dependence of growth and faceting of manganese-doped GaN nanowires. *J Am Chem Soc* 129: 10980–10981.
10. Berger LI (1997) *Semiconductor Materials*, CRC Press.
11. Assali S, Zardo I, Plissard S, et al. (2013) Direct band gap wurtzite gallium phosphide nanowires. *Nano Lett* 13: 1559–1563.
12. Hara T, Akasaki I (1968) Electrical properties of sulfur-doped gallium phosphide. *J Appl Phys* 39: 285–289.
13. Liu C, Sun J, Tang J, et al. (2012) Zn-doped p-type gallium phosphide nanowire photocathodes from a surfactant-free solution synthesis. *Nano Lett* 12: 5407–5411.
14. Zeng ZM, Li Y, Chen JJ, et al. (2008) GaP/GaO_x core-shell nanowires and nanochains and their transport properties. *J Phys Chem C* 112: 18588–18591.
15. Lyu SC, Zhang Y, Ruh H, et al. (2003) Synthesis of high-purity GaP nanowires using a vapor deposition method. *Chem Phys Lett* 367: 717–722.
16. Gu Z, Paranthaman MP, Pan Z (2009) Vapor-phase synthesis of gallium phosphide nanowires. *Cryst Growth Des* 9: 525–527.
17. Liu BD, Bando Y, Tang CC, et al. (2005) Synthesis of GaP nanowires with Ga_2O_3 coating. *Appl Phys A* 80: 1585–1588.
18. Cerqueira CF, Viana BC, da Luz-Lima C, et al. (2015) (Ga, In)P nanowires grown without intentional catalyst. *J Cryst Growth* 431: 72–78.
19. Kuyanov P, Boulanger J, LaPierre RR (2017) Control of GaP nanowire morphology by group V flux in gas source molecular beam epitaxy. *J Cryst Growth* 462: 29–34.
20. Elena H, Daniele E, Mauro G, et al. (2014) Growth of defect-free GaP nanowires. *Nanotechnology* 25: 205601.
21. Kornienko N, Whitmore DD, Yu Y, et al. (2015) Solution phase synthesis of indium gallium phosphide alloy nanowires. *ACS Nano* 9: 3951–3960.
22. Hosein ID, Hegde M, Jones PD, et al. (2014) Evolution of the faceting, morphology and aspect ratio of gallium oxide nanowires grown by vapor–solid deposition. *J Cryst Growth* 396: 24–32.

23. Pan ZW, Dai ZR, Wang ZL (2001) Nanobelts of semiconducting oxides. *Science* 291: 1947–1949.
24. Hu J, Odom TW, Lieber CM (1999) Chemistry and physics in one-dimension: Synthesis and properties of nanowires and nanotubes. *Accounts Chem Res* 32: 435–445.
25. Gupta R, Xiong Q, Mahan GD, et al. (2003) Surface optical phonons in gallium phosphide nanowires. *Nano Lett* 3: 1745–1750.
26. Dobrovolsky A, Sukrittanon S, Kuang YJ, et al. (2014) Raman spectroscopy of GaP/GaNP core/shell nanowires. *Appl Phys Lett* 105: 193102.
27. de la Chapelle ML, Han HX, Tang CC (2005) Raman scattering from GaP nanowires. *Eur Phys J B* 46: 507–513.

AIMS Press